Chapter 14

Medical Applications of Nuclear Technology

The exploitation of nuclear technology in medical applications began almost from the moment of Roentgen's discovery of x rays in 1895 and Becquerel's discovery of radioactivity in 1996.[1] The importance of x rays in medical diagnosis was immediately apparent and, within months of their discovery, the bactericidal action of x rays and their ability to destroy tumors were revealed. Likewise, the effectiveness of the newly discovered radioactive elements of radium and radon in treatment of certain tumors was discovered early and put to use in medical practice. Today, both diagnostic and therapeutic medicine as well as medical research depend critically on many clever and increasingly sophisticated applications of nuclear radiation and radioisotopes.

In diagnostic medicine, the radiologist's ability to produce images of various organs and tissues of the human body is extremely useful. Beginning with the use of x rays at the start of the twentieth century to produce shadowgraphs of the bones on film, medical imaging technology has seen continuous refinement. By the 1920s, barium was in use to provide contrast in x-ray imaging of the gastrointestinal system. Intravenous contrast media such as iodine compounds were introduced in the 1930s and in angiography applications by the 1940s. Fluoroscopic image intensifiers came into use in the 1950s and rare-earth intensifier screens in the 1960s. Computed tomography (CT), positron emission tomography (PET), and single-photon emission tomography (SPECT) saw their beginnings for clinical use in the 1960s and 1970s. Picture archive and communication systems (PACS) began to see common use in the 1990s. The 1990s also saw interventional radiology becoming well established in medical practice, especially in coronary angioplasty procedures.

Along with advances in diagnostic medicine, corresponding advances have been made in using nuclear technology for therapy. There are three general classes of radiation therapy. In *brachytherapy*, direct implants of a radioisotope are made into a tumor to deliver a concentrated dose to that region. In *teletherapy*, a beam delivers radiation to a particular region of the body or even to the whole body. In *radionuclide therapy*, unsealed radiopharmaceuticals are directly administered to patients for curative or palliative purposes.

---

[1] The history of medical uses of radiation from 1895 through 1995 is addressed thoroughly in a series of articles published in the November 1995 issue of *Health Physics*, the Radiation Protection Journal.

Table 14.1. Global use of medical radiology (1991-1996). From UN [2000].

Quantity		No. per 10^6 population Level I[a]	Global
Physicians			
All physicians		2800	1100
Radiological physicians		110	80
X-ray Imaging			
Equipment:	medical	290	110
	dental	440	150
	mammography	24	7
	CT	17	6
Exams per year:	medical	920,000	330,000
	dental	310,000	90,000
Radionuclide Imaging			
Equipment:	gamma cameras	7.2	2.1
	rectilinear scanners	0.9	0.4
	PET scanners	0.2	0.05
Exams per year		19,000	5600
Radionuclide Therapy			
Patients per year:		170	65
Teletherapy			
Equipment:	x-ray	2.8	0.9
	radionuclide	1.6	0.7
	LINAC	3.0	0.9
Patients per year		1500	820
Brachytherapy			
Afterloading units		1.7	0.7
Patient per year		200	70

[a] Level I represents countries with one or more physicians per 1000 population.

Indeed, nuclear applications have become such a routine part of modern medical practice that almost all of us at one time or another have encountered some of them. Table 14.1 lists personnel and frequencies for medical radiology and radiation therapy procedures, both globally and in developed countries.

Today we see many changes and new applications of nuclear technology in medicine. The use of rectilinear scanners is declining rapidly while the use of gamma-ray cameras, PET and CT scanners is growing. Diagnostic radiology has long been used

for imaging and study of human anatomy. In recent years, using CT, PET, and gamma-ray scanners, as well as MRI (magnetic resonance imaging), medical science has advanced to imaging the physiology and metabolism of the human body.

14.1 Diagnostic Imaging

Diagnostic radiology using x rays, both dental and medical, including mammography, dominates radiology. This is true for both numbers of patients and numbers of procedures. Each year in the United States, for example, more than 130 million persons annually receive diagnostic x rays [NAS 1980] and more than 250 million examinations are performed [UN 2000].

In the past thirty years, alternatives to traditional x-ray imaging have become available and are being increasingly used to image organs and tissues not easily seen by conventional x-ray diagnostics. In the 1970s, digital methods of processing and displaying x-ray images led to the clinical use of digital radiology and computed tomography (CT). Positron emission tomography (PET), and single photon emission computed tomography (SPECT), both radiological procedures, were realized in the 1980s.

Magnetic resonance imaging (MRI) matured and became a widely used medical imaging technique in the 1990s. MRI does not use x rays or radionuclides; however, it does depend on the unique spin (angular momentum) properties of the atomic nuclei in the body tissues and also employs the sophisticated image processing techniques used in nuclear imaging methods. Indeed, PET and MRI or PET and CT are often used together, with images superimposed to reveal physiological processes, particularly in the brain.

14.1.1 X-Ray Projection Imaging

Projection x-ray imaging is by far the most common diagnostic imaging technique used. In this method, a beam of x rays illuminates some part of the body and a film (or digital imaging detector) behind the body records the transmitted x rays. Areas of the film behind dense high-Z materials such as bone, which preferentially absorb x rays, receive little exposure on the film compared to areas behind soft tissue, which more readily transmit the photons. In essence, an x-ray image records the "shadows" cast or *projected* by the irradiated specimen onto the film.

During the fifty years following the discovery of x rays, advances were made in the design and standardization of x-ray sources, and in the use of contrast agents. Notable advances in design include the 1913 invention of the hot-cathode x-ray tube by William Coolidge, the invention of the anti-scatter grid by Gustav Bucky and H.E. Potter in 1917, and the invention of the x-ray image intensifier by John Coltman in 1948 [Webster 1995]. Contrast agents are fluids containing high-Z atoms that strongly absorb x rays compared to normal tissues. Barium compounds flooding the gastrointestinal system were found to give definition in an x-ray image of the volume of the system. After clearance and distention of the system by gas, residual barium defined the walls of the system. Similarly, iodine compounds in the blood were found to define the circulatory system in detail. Advances continue to be made in the availability of contrast agents and in their applications. Film subtraction angiography, which began in the 1930s, relies on contrast agents. Subtraction

angiography requires two images, one positive, one negative, recorded before and after injection of a contrast agent. Subtraction of the images by superimposing the two film images reveals vascular structure, absent interference caused by superposition of extraneous images of bones and other structures. In recent decades, digital-imaging methods have greatly enhanced the effectiveness of this application by performing the subtraction digitally.

The X-Ray Source

The production of x-ray photons as bremsstrahlung and fluorescence occurs in any device that produces high-energy electrons. Devices that can produce significant amounts of x rays are those in which a high voltage is used to accelerate electrons, which then strike an appropriate target material. Such is the basic principle of all x-ray tubes used in medical diagnosis and therapy, industrial applications, and research laboratories.

Although there are many different designs of x-ray sources for different applications, most designs for low to medium voltage sources ($\lesssim 180$ kV) place the electron source (cathode) and electron target (anode) in a sealed glass tube. The glass tube acts as both an insulator between the anode and cathode and a container for the necessary vacuum through which the electrons are accelerated by the high voltage between the anode and cathode. The anodes of x-ray tubes incorporate a suitable metal upon which the electrons impinge and generate bremsstrahlung and characteristic x rays. Most of the electron energy is deposited in the anode as heat rather than being radiated away as x rays and, thus, heat removal is an important aspect in the design of x-ray tubes. For example, the x-ray tube shown in Fig. 14.1 has a rotating anode that spreads the heat over a large area and thereby allows higher beam currents and greater x-ray output.

Tungsten is the most commonly used target material because of its high atomic number and because of its high melting point, high thermal conductivity, and low vapor pressure. Occasionally, other target materials are used when different characteristic x-ray energies are desired (see Table 14.2). Generally, the operating conditions of a particular tube (current, voltage, and operating time) are limited by the rate at which heat can be removed from the anode. For most medical and dental diagnostic units, voltages between 40 and 150 kV are used, while medical therapy units may use 6 to 150 kV for superficial treatment or 180 kV to 50 MV for treatment requiring very penetrating radiation.
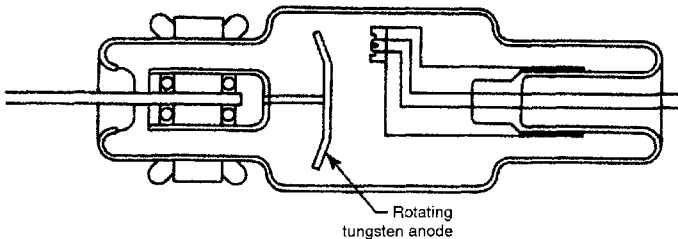

Rotating
tungsten anode

Figure 14.1. Schematic diagram of a typical x-ray tube. From Kaelble (1967).

Table 14.2. Characteristic x-ray properties of two important target materials used in x-ray tubes. The x-ray line notation refers to the specific electron transition to the K or L shell that produces the characteristic x ray. The wavelength and energy of the resulting characteristic x ray is listed. The excitation voltage is the energy required to create (ionize) a shell vacancy whose repopulation generates the x ray.

Element	X-ray line	Wavelength $(10^{-10}$ m)	Energy (keV)	Excitation voltage (kV)
Tungsten	$K_{\alpha 1}$	0.2090	59.3182	69.525
	$K_{\beta 1}$	0.1844	67.2443	69.525
	$L_{\alpha 1}$	1.4764	8.3976	10.207
	$L_{\beta 1}$	1.2818	9.6724	11.514
Molybdenum	$K_{\alpha 1}$	0.7093	17.4793	20.000
	$K_{\beta 1}$	0.6323	19.6083	20.000
	$L_{\alpha 1}$	5.4066	2.2932	2.520

The energy spectrum of x-ray photons emitted from an x-ray tube has a continuous bremsstrahlung component up to the maximum electron energy (i.e., the maximum voltage applied to the tube). If the applied voltage is sufficiently high as to cause ionization in the target material, there will also be characteristic x-ray lines superimposed on the continuous bremsstrahlung spectrum. In Fig. 14.2 two calculated exposure spectra of x rays are shown for the same operating voltage but for different amounts of beam filtration (i.e., different amounts of material attenuation in the x-ray beam). As the beam filtration increases, the low-energy x rays are preferentially attenuated and the x-ray spectrum hardens and becomes more penetrating. Also readily apparent in these spectra are the tungsten $K_{\alpha 1}$ and $K_{\beta 1}$ characteristic x rays.

The characteristic x rays may contribute a substantial fraction of the total x-ray emission. For example, the L-shell radiation from a tungsten target is between 20 and 35% of the total energy emission when voltages between 15 and 50 kV are used. Above and below this voltage range, the L component rapidly decreases in importance. However, even a small degree of filtering of the x-ray beam effectively eliminates the low-energy portion of the spectrum containing the L-shell x rays. The higher-energy K-series x rays from a tungsten target contribute a maximum of 12% of the total x-ray exposure for operating voltages between 100 and 200 kV [ICRU 1970].

The X-Ray Receiver
The receiver in x-ray projection imaging is normally a film cassette, although photostimulable phosphor plates, with digital output, have seen growing use since the 1980s. Within the cassette is a film sheet with a polyester base and silver halide emulsion on one or both sides. Likewise, on one or both sides is found a fluorescent screen which absorbs the x rays and emits visible light matched to the sensitivity of the emulsion. The screen most frequently used from 1896 through the 1970s is $CaWO_4$, which typically stops 20 to 40% of the x rays. In recent years screens made of lanthanum, gadolinium, and yttrium compounds have come into use. These
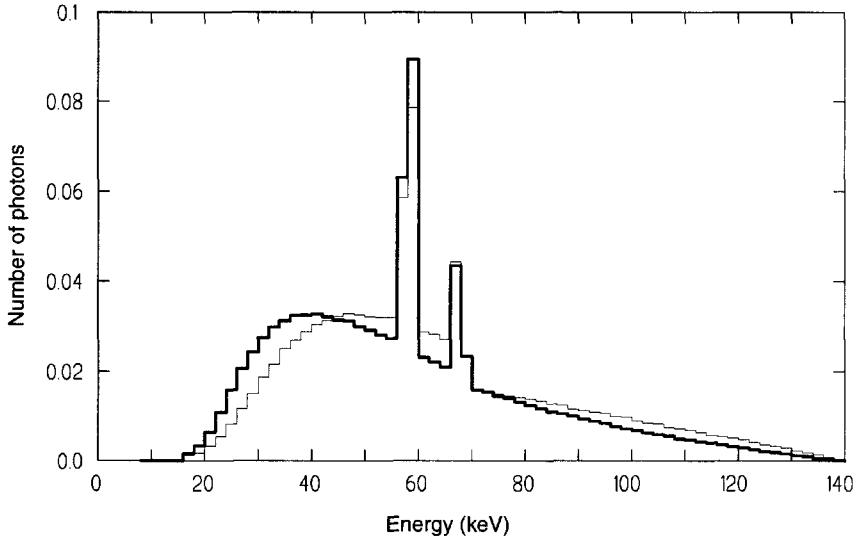
Figure 14.2. Measured photon spectra from a Machlett Aeromax x-ray tube (tungsten anode) operated at a constant 140 kV potential. This tube has an inherent filter thickness of 2.50-mm aluminum equivalent and yields a spectrum (thick line) with a HVL quality of 5.56-mm Al equivalent. The addition of an external 6-mm aluminum filter hardens the spectrum (thin line) to a HVL quality of 8.35-mm Al equivalent. Both spectra are normalized to unit area. Data are from Fewell, Shuping, and Hawkins (1981).

screens, which absorb 40 to 60% of the x rays, greatly improves sensitivity and typically reduces patient doses by a factor of 50.

Contrast in the X-Ray Image

A basic, ideal measure of contrast is the *subject contrast* associated with the visibility of a feature in the x-ray subject. This is illustrated in Fig. 14.3. The subject is irradiated with a parallel beam of x rays with intensity I_o, which are either stopped, scattered or reach the receiver without interaction. From Eq. (7.4), uncollided rays that reach the receiver without passing through the feature have an intensity
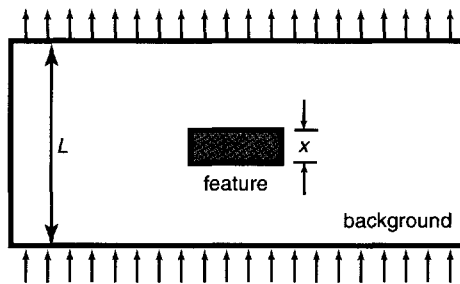

Figure 14.3. Background space of thickness L containing a feature of thickness x exposed to a parallel beam of x rays.

$I_b = I_o \exp[-\mu_b L]$ where μ_b is the effective linear attenuation coefficient for the background material. Uncollided rays that pass through the feature of thickness x and a thickness $L - x$ of background material have an intensity $I_f = I_o \exp[-(L - x)\mu_b - \mu_f x]$, where μ_f is the effective linear attenuation coefficient for the feature material. The subject contrast is defined as

$$C_s \equiv \frac{I_b - I_f}{I_b} = 1 - \frac{I_f}{I_b} = 1 - \exp[-(\mu_f - \mu_b)x]. \qquad (14.1)$$

To a first approximation, the attenuation coefficient is proportional to the density of the material and only very secondarily dependent on the energy spectra of the x rays. Thus,

$$C_s = 1 - \exp\left(\left[\left(\frac{\mu}{\rho}\right)_b \rho_b - \left(\frac{\mu}{\rho}\right)_f \rho_f\right] x\right). \qquad (14.2)$$

Values of μ/ρ are relatively insensitive to material, so the subject contrast depends primarily on relative densities. For example, for 100-keV x rays, μ/ρ (cm^2/g) varies from 0.149 for air to 0.164 for tissue or water, to 0.175 for bone, while densities vary from 0.0012 g/cm^3 for air to 1.0 for tissue, to about 1.85 for bone. For a 1-cm thickness of bone in tissue, the contrast would be about 15%. Very dense substances such as barium or iodine are excellent choices for contrast agents, not only because of their relatively high densities but also because of the greater photoelectric absorption of x rays in these high-Z materials.

Image contrast is less than subject contrast for several reasons. One is the contribution of scattered x rays to the "background." For this reason, and also to minimize patient exposure, the x-ray field of view should be kept to a minimum. At low exposures, statistical variations in the x-ray fluence at the image result in "quantum mottle" in the image. Loss of contrast due to scattered x rays can be reduced greatly by the use of an *antiscatter grid* adjacent to the receiver. Such a grid consists of alternating slats of lead and a low-Z filler material such as carbon fiber or aluminum, oriented so as to collimate the uncollided x ray beam through the filler and to absorb in the lead the scattered x rays, which mostly travel in directions other than the direction of the primary beam. Because the slats can yield structure in the image, the grid is sometimes placed in motion during the x-ray exposure. Grids are characterized by the number of slats (lines) per inch or per cm, and by the grid ratio, the ratio of the height (attenuation thickness) of the slats to the distance separating them.

14.1.2 Fluoroscopy

There are many circumstances calling for viewing the x-ray image in real time or for recording a time sequence of images. Examples include the placement of catheters in coronary artery angioplasty and the observation of peristalsis in the gastrointestinal system. Fluoroscopy procedures involve lower dose rates than those used in film imaging, but greater total patient doses.

In early years, radiologists directly viewed fluorescent-screen receivers in darkened rooms, a process requiring dark-adapted eyes and long exposures. Indeed, conventional photographic images were sometimes taken of the screen images. In

the 1950s, invention of the image intensifier revolutionized fluoroscopy. In the intensifier, the transmitted x-ray beam strikes a thin input phosphor plate, typically CsI 9 to 13 in. square. Visible light is emitted from this phosphor, with many photons released per x ray absorbed. The visible light, in turn, falls on a photocathode, typically SbS_3, which releases photoelectrons. These electrons are accelerated and focused onto an output phosphor, typically 1-in. square ZnCdS(Ag), which is viewed by a video camera, and, using a beam splitter, photographed on conventional 35-mm movie film.

14.1.3 Mammography

The use of x rays to screen for malignancies of the breast is technically very demanding. Two features are of interest: microcalcifications that are sometimes indicative of cancer, and actual tumors a fraction of a cm in size, usually in lymphatic tissue, and with a composition similar to the surrounding breast tissue. Microcalcification imaging requires high resolution and tumor imaging requires high contrast. Breast compression improves resolution and, ideally, low-energy and nearly monoenergetic x rays would be used. This is approached by using an x-ray anode such as Mo, and by restricting the electron beam to a very small focal spot on the anode. The first practical work in mammography dates from the introduction of the Mo target by Gros in 1995. This and other advances are described by Hendee [1995]. From Table 14.2 we see the K-shell x rays for Mo have energies of 17.5 and 19.6 keV, and the K-shell binding energy is about 20 keV. A Mo filter is then placed in the x-ray beam. This filter passes the K-shell x rays but attenuates those of higher or lower energy. Thus, the beam reaching the breast consists mostly of characteristic x rays. To increase resolution, single-emulsion films are used with single intensifying screens. Grids with 30-50 lines per cm and 5:1 ratios are also used to substantially improve contrast by reducing the scattered radiation reaching the film.

14.1.4 Bone Densitometry

Monitoring of bone density is essential in the diagnosis and treatment of osteoporosis and related disorders. Several methods are available to measure bone density, but the most widely used technique is dual energy x-ray absorptiometry (DEXA). Other techniques include ultrasound and quantitative computed tomography (see subsequent sections). DEXA is thought to be more reproducible and more able to predict bone strength. DEXA, which involves an x-ray beam containing photons of two distinct energies, has largely replaced dual photon absorptiometry (DPA), which involves a low-energy gamma ray source with two distinct energies. An example is ^{153}Gd, which emits 44 and 100-keV photons.

In measurement of bone mass with a DEXA machine, the patient rests on a flat padded table and remains motionless while the "arm" of the instrument passes over the whole body or over selected areas. A beam of x rays, of two energies, passes from below the table through the area being measured. These x-rays are detected by a device in the instrument's arm. The machine converts the information received by the detector into an image of the skeleton and analyzes the quantity of bone the skeleton contains. The results are usually reported as bone mineral density (BMD), the amount of bone per unit of skeletal area.

Consider a subject region containing bone, with mass thickness $\rho_b x_b$ and soft tissue, with mass thickness $\rho_s x_s$, perpendicular to the dual beam, with incident intensities identified respectively as I_{1o} and I_{2o}. The two transmitted beams would have the following uncollided intensities after attenuation:

$$I_1 = I_{1o} \exp\left[-\left(\frac{\mu_1}{\rho}\right)_b \rho_b x_b - \left(\frac{\mu_1}{\rho}\right)_s \rho_s x_s \right], \tag{14.3}$$

$$I_2 = I_{2o} \exp\left[-\left(\frac{\mu_2}{\rho}\right)_b \rho_b x_b - \left(\frac{\mu_2}{\rho}\right)_s \rho_s x_s \right]. \tag{14.4}$$

From these equations, the unknown mass thickness of the bone may be computed as

$$\rho_b x_b = \frac{\mathcal{R}\ln[I_1/I_{1o}] - \ln[I_2/I_{2o}]}{(\mu_2/\rho)_b - \mathcal{R}(\mu_1/\rho)_s}, \tag{14.5}$$

in which $\mathcal{R} \equiv (\mu_2/\rho)_s / (\mu_1/\rho)_s$.

14.1.5 X-Ray Computed Tomography (CT)

X-ray tomography produces a two-dimensional cross sectional image of an object from x-ray transmission data consisting of projections of the cross section collected from many directions. Consider the cross section shown in Fig. 14.4. Suppose the object is traversed by x rays in a uniform, parallel beam in the plane of the cross section. X-ray computed tomography (CT) generates an image of the *object function* $f(x, y) \equiv \mu(x, y)$, the effective linear attenuation coefficient of the material at position (x, y). Three dimensional images may be generated from successive plane slices.

Suppose the x-ray beam travels along direction s, normal to the projection-traverse direction t and at angle θ to the x axis. The relation between the (s, t) rotated coordinated system and the original (x, y) coordinate system is

$$t = x\cos\theta + y\sin\theta \quad \text{and} \quad s = -x\sin\theta + y\cos\theta. \tag{14.6}$$

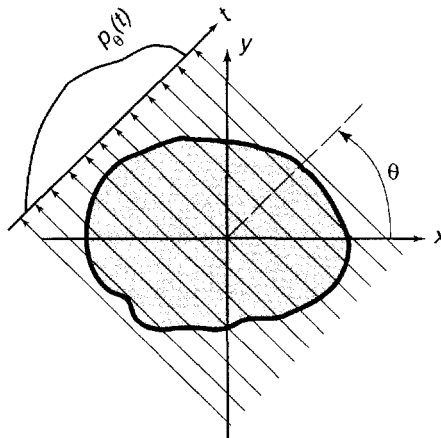**Figure 14.4.** Plane cross section with the object function $f(x, y)$, and the projection generated by a parallel beam of x rays at angle θ.

If I_o is the intensity of the incident beam, then the intensity of uncollided photons passing through the object plane at transverse distance t and angle θ is

$$I_\theta(t) = I_o \exp\left[-\oint ds f(x(s), y(s))\right].\tag{14.7}$$

where $\oint ds\, f$ is the line-integral of μ along the ray s that intersects the projection axis at t. Sometimes this integral is called the optical thickness, and represents the number of mean-free-path lengths an uncollided photon must traverse to reach t. The projection data used to construct an image of $f(x, y)$ is

$$p_\theta(t) \equiv -\ln\left[\frac{I_\theta(t)}{I_o}\right] = \oint ds f(x(s), y(s))$$

$$= \int_{-\infty}^{\infty} dx \int_{-\infty}^{\infty} dy\, f(x, y)\delta(x\cos\theta + y\sin\theta - t).\tag{14.8}$$

The challenge of CT is to reconstruct $f(x, y)$ from a set of projections $p_\theta(t)$, each one taken at a different value of θ. Implementation of a practical CT scanner dates from the efforts of Hounsfield and Cormack, working independently, who shared the Nobel prize in 1972 for their work.

Of critical importance to image reconstruction is the Fourier transform which converts spatial domain data into spatial frequency data. The one-dimensional transform and its inverse are defined as

$$F(\omega) = \mathcal{F}_1[f(x)] = \int_{-\infty}^{\infty} dx\, f(x)e^{+j2\pi\omega x},\tag{14.9}$$

$$f(x) = \mathcal{F}_1^{-1}[F(\omega)] = \int_{-\infty}^{\infty} d\omega\, F(\omega)e^{-j2\pi\omega x}.\tag{14.10}$$

Similarly, the two-dimensional Fourier transform is used to convert (x, y) data into spatial frequency (u, v) data, namely

$$F(u, v) = \mathcal{F}_2[f(x, y)] = \int_{-\infty}^{\infty} dx \int_{-\infty}^{\infty} dy\, f(x, y)e^{+j2\pi(ux+vy)}.\tag{14.11}$$

$$f(x, y) = \mathcal{F}_2^{-1}[F(u, v)] = \int_{-\infty}^{\infty} du \int_{-\infty}^{\infty} dv\, F(u, v)e^{-j2\pi(ux+vy)}.\tag{14.12}$$

Image Reconstruction by Filtered Backprojection

The filtered backprojection algorithm (called the convolution backprojection algorithm) is the most popular and most frequently used technique for constructing an image from projection data. This method is based on the slice or projection theorem, which relates a projection to a "slice" of the two-dimensional Fourier transform $F(u, v)$ of the object function. To obtain this key relationship take the 1-D Fourier transform of $p_\theta(t)$, as given by Eq. (14.8), namely,

$$P_\theta(\omega) = \mathcal{F}_1[p_\theta(t)] = \int_{-\infty}^{\infty} dt\, p_\theta(t)e^{+j2\pi\omega t}$$

$$= \int_{-\infty}^{\infty} dt\, e^{+j2\pi\omega t} \int_{-\infty}^{\infty} dx \int_{-\infty}^{\infty} dy\, f(x,y)\delta(x\cos\theta + y\sin\theta - t).$$

$$= \int_{-\infty}^{\infty} dx \int_{-\infty}^{\infty} dy\, f(x,y)e^{2\pi j(x\omega\cos\theta + y\omega\sin\theta)}$$

$$= F(u,v)\bigg|_{\theta} = F(\omega,\theta). \tag{14.13}$$

Here $F(u,v)$ is the 2-D Fourier transform of $f(x,y)$, and $u = \omega\cos\theta$ and $v = \omega\sin\theta$ are the spatial frequencies. The pairs (u,v) and (ω,θ) thus represent the Cartesian and polar coordinates of (x,y) in the spatial frequency domain.

This projection theorem, which is central to 2-D image reconstruction, shows that a 1-D Fourier transform of the projection data for a given value of θ yields a slice of the 2-D Fourier transform of $f(x,y)$ in the frequency domain along a frequency radius $u = \omega\cos\theta$ and $v = \omega\sin\theta$. With values of $F(u,v)$ obtained from this theorem, the object functions can be recovered by taking a 2-D inverse Fourier transform of $F(u,v)$, i.e.,

$$f(x,y) = \int_{-\infty}^{\infty} du \int_{-\infty}^{\infty} dv\, F(u,v)e^{-j2\pi(ux+vy)}, \tag{14.14}$$

which, in polar frequency coordinates, can be written as

$$f(x,y) = \int_{0}^{2\pi} d\theta \int_{-\infty}^{\infty} d\omega\, |\omega| F(\omega,\theta)e^{-j2\pi\omega(x\cos\theta + y\sin\theta)}. \tag{14.15}$$

Since $t = x\cos\theta + y\sin\theta$ and with Eq. (14.13) used to express $F(u,v)$ in terms of the projection data p_θ, we can rewrite this result as

$$f(x,y) = \int_{0}^{2\pi} d\theta \int_{-\infty}^{\infty} d\omega\, |\omega| \left\{ \int_{-\infty}^{\infty} dt'\, p_\theta(t')e^{+j2\pi\omega t'} \right\} e^{-j2\pi\omega(x\cos\theta + y\sin\theta)}.$$

$$= \int_{0}^{2\pi} d\theta \int_{-\infty}^{\infty} dt'\, p_\theta(t')g(t - t'), \tag{14.16}$$

where $g(\tau) \equiv \int_{-\infty}^{\infty} d\omega\, |\omega| e^{-j2\pi\omega\tau} = \mathcal{F}_1^{-1}[|\omega|]$. Finally, the projection data has the symmetry $p_\theta(t) = p_{\theta+\pi}(t)$, so that Eq. (14.16) can be written as

$$\boxed{f(x,y) = \int_{0}^{\pi} d\theta \int_{-\infty}^{\infty} dt'\, \widehat{p}_\theta(t')g(t - t'),} \tag{14.17}$$

with $\widehat{p}_\theta(t') = p_\theta(t') + p_{\theta+\pi}(t')$ and $t = x\cos\theta + y\sin\theta$.

The convolution kernel $g(\tau)$ in Eq. (14.17) is an inverse Fourier transform of $|\omega|$, whose exact form cannot be achieved in practice. Consequently, several different filter functions are used to obtain numerical results, each with its own resolution and contrast characteristics. Finally, the above equations have been written as though

data were continuous in the dependent variables, and without noise or error. In fact, data are digital and not without uncertainty. Many methods are available for generating $f(x, y)$ from projections $P_\theta(t)$. As advances are made in computing power and parallel processing methods, even more algorithms will become available for reconstruction of images from projection data.

Fan-Beam CT

The parallel-beam projection geometry just described is very cumbersome and not very practical. For each angle θ, both the source and the detector must move. Large scanning times are required, and there is undue patient exposure to x rays. In fan-beam tomography, the x-ray beam is collimated to a thin fan-shaped beam of rays, which pass through the object and are received in an array of detectors in the plane of the beam. Typically, source and detectors would be on the perimeter of a circle, with detectors subtending equal solid angles from the source. Both source and detectors then rotate about the object to obtain projection data at different angles. Figure 14.5 shows the fan-beam x-ray source in the GE HiSpeed Advance CT and Fig. 14.6 shows the array of detectors used in this device. Fan-beam tomography was introduced in 1973.
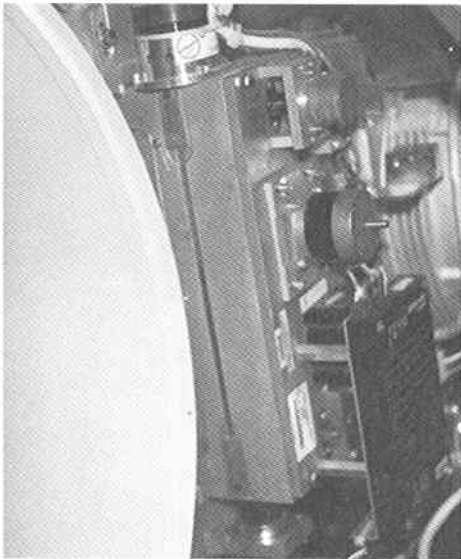

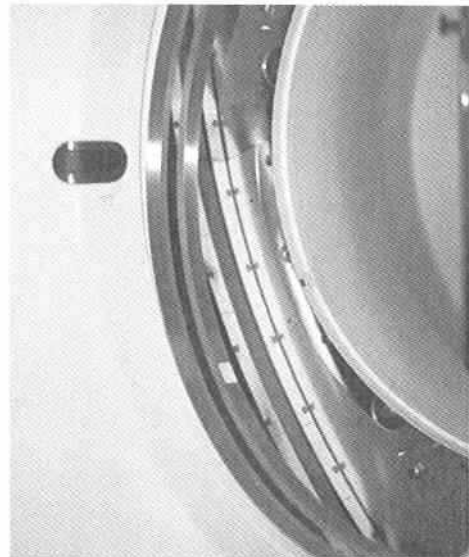
Figure 14.5. GE HiSpeed Advance CT x-ray source.

Figure 14.6. GE HiSpeed Advance CT x-ray receiver.

Spiral CT

In fan-beam CT, a series of slices are imaged, with the object translated axially a few mm between successive slices. Individual slice thicknesses are 2 to 10 mm. Each slice may be imaged in about a second, but tens of seconds are required for translation and preparation. In thorax imaging the breath must be held for each slice, but uneven breathing yields differences between images and artifacts in 3-D volume reconstruction. Thorax imaging is thus difficult and angiography procedures

are precluded [Hiriyannaiah 1997]. In spiral CT, which was introduced in 1989 there is continuous rotation of the source and continuous translation of the object normal to the (x, y) image plane. It is possible to scan the entire thorax or abdomen in one breath hold, in a fraction of a minute. With this technique, it is possible to generate 3-D images very nearly isotropic in voxel (3-D pixel) size. Figure 14.7 illustrates a modern spiral CT scanner used in diagnostic radiology and in treatment planning for radiation therapy. The left panel of Fig. 14.15 illustrates a CT scan of the thorax region. In the right panel, a merged PET and CT scan of the thorax is shown. This figure is explained in the discussion of PET scanning.
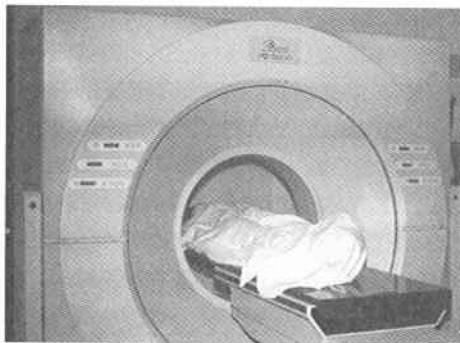

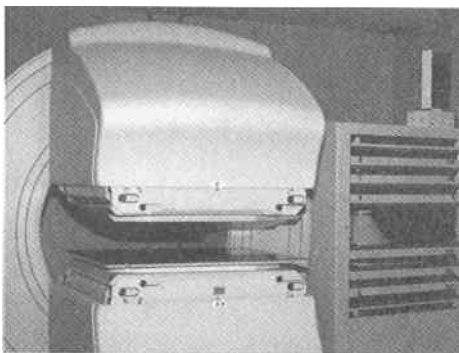**Figure 14.7.** Marconi Medical System PQ5000 continuous spiral CT scanner.

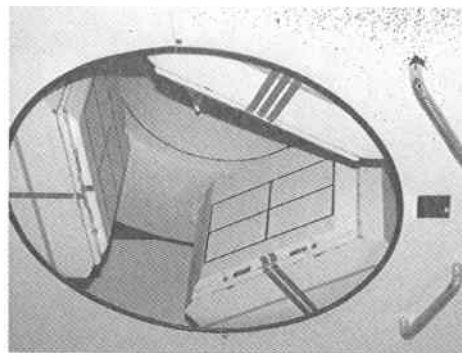**Figure 14.8.** Two-headed SPECT scanner.

Figure 14.9. Three-headed SPECT scanner.

14.1.6 Single Photon Emission Computed Tomography (SPECT)

The goal of SPECT is the determination of the 3-D spatial distribution within the body of a radiopharmaceutical administered to a patient. Because a radiopharmaceutical concentrates in regions in which it undergoes biological use, SPECT is capable of measuring quantitatively biological and metabolic functions in the body. This is in contrast to CT which primarily produces images of anatomical structures in the human body.

The radionuclide used as a tag in the administered pharmaceutical emits a gamma ray upon its radioactive decay. Frequently used radioisotopes include ^{99m}Tc, ^{125}I and ^{131}I, all widely used in nuclear medicine. The basic idea behind SPECT is very similar to CT. At some detector plane, the intensity of uncollided gamma rays leaving the body in a well defined direction is recorded. By moving the detector plane around the subject, gamma-ray emission projections are obtained at many different angles. From these projections, the spatial distribution of the radionuclide activity in the body can be obtained in much the same way as the x-ray projections in CT are used to reconstruct an image of the different materials in the body.

SPECT was first developed in 1963 by Kuhl and Edwards, well before x-ray CT and the advent of modern tomographic image reconstruction methods. Since then, the method has been considerably extended by the use of the gamma camera, invented by Anger. Today SPECT machines with up to four gamma cameras rotating around the patient are available. Work continues on improving both the sensitivity and resolution of this imaging technology.

The Gamma Camera

Central to SPECT is a so-called *gamma camera* which detects the gamma rays emitted from within the patient. The gamma camera consists of a NaI(Tl) scintillator crystal, circular or rectangular in shape, with a collimator on the side facing the patient and an array of photomultiplier tubes, optically coupled to the crystal, on the other side. Circular crystals are typically 25 to 50 cm in diameter; rectangular crystals have sides of 15 to 50 cm. Thickness is typically 1/4 to 5/8 in., with 3/8 in. being most common. Thin crystals provide the best resolution; but for imaging with high energy gamma rays or 0.511-MeV annihilation photons, the greater efficiency of a thicker crystal is often needed.

As many as 100 photomultiplier tubes are used in the array. Each has a different response (pulse height output) resulting from a scintillation event at position (x, y) in the crystal plane. A weighted average of the responses (Anger position logic) yields the (x, y) coordinates of the event in the crystal. Pulse height discriminators are used, with a 15 to 20% window set to record events corresponding to photoelectric absorptions in the crystal from uncollided source photons. In this way, preponderantly uncollided photons coming from the patient are recorded. This energy discrimination, along with use of the front-end collimator, minimizes "out of focus" registration of events caused by photons that have scattered one or more times in the body of the patient. Figure 14.8 shows a SPECT scanner with two cameras and Fig. 14.9 shows a three-camera scanner.

Collimators

The position logic used to register the location of a gamma-ray event in the scintillator crystal establishes an intrinsic spatial resolution R_I of 2.5 to 4.5 mm. However, to identify the site in the patient where the gamma ray originated requires the use of a collimator. The simplest and earliest used is a pinhole collimator (see Fig. 14.10). With a pinhole diameter d, distances f and b from the pinhole to the image and object plane, and image diameter I, the image magnification is $M = f/b$, and the point-spread, i.e., the image width of a point emitting photons, is $R_{ph} = (d/f)(f + b)$. The system resolution, accounting for both intrinsic resolution
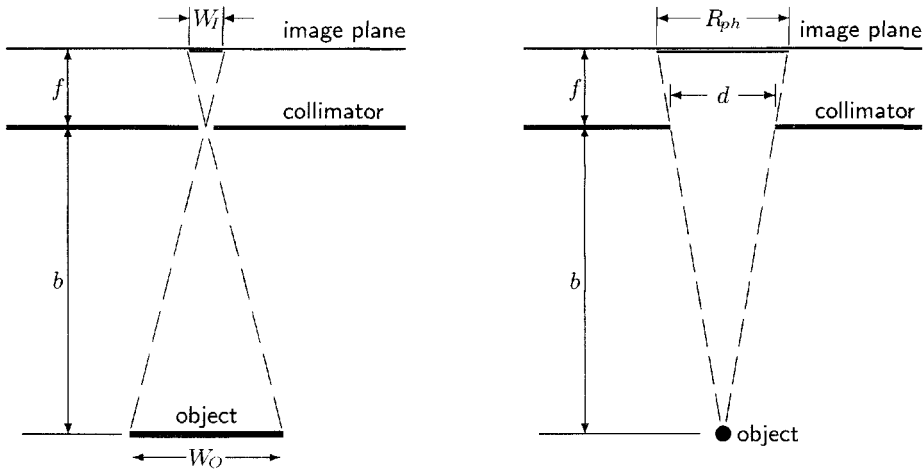
Figure 14.10. Left: The magnification of an object produced by a pin-hole collimator is $\equiv W_I/W_O = f/b$. Right: The resolution R_{ph} of a pin-hole collimator is given by $R_{ph}/(f + b) = d/b$ or $R_{ph} = (d/b)/(f + b)$.

and the point spread, is

$$R_{sys} = \sqrt{R_{ph}^2 + (R_I/M)^2}. \tag{14.18}$$

Because a pinhole collimator has very poor sensitivity as a result of the relatively few photons admitted to the NaI scintillator, a parallel-hole collimator is more frequently used. This collimator has densely packed tubes, usually hexagonal in shape and perpendicular to the detector surface, with absorbing walls that ideally absorb all gamma rays except those that travel in the direction of the tubes. With a the thickness of the collimator (hole length), b the source to collimator distance, c the distance from the collimator to the point of interaction in the crystal, and d the effective diameter of the collimator hole, the collimation point-spread resolution is $R_{ph} = (d/a)(a+b+c)$, and the system resolution is as above. The system resolution may be improved by reducing d, reducing c, and/or reducing b. However, improving the resolution decreases the sensitivity, and collimators are designed to be either high resolution or high sensitivity. Focusing collimators, converging or diverging holes, are also used to better match the image size to the size of the organ being imaged. Focal length as well as sensitivity versus resolution are important choices in the selection of focusing collimators.

Image Reconstruction

Suppose $f(x,y)$ in Fig. 14.4 represents the activity distribution in the (x,y) object plane. Multiple projections $p_\theta(t)$ are gathered singly or simultaneously for successive object planes, i.e., for different values of θ. Reconstruction of the spatial activity distribution from the projections generally makes use of the filtered backprojection algorithm. However, this reconstruction process is complicated because of the need to compensate for three-dimensional effects of attenuation and scatter of

photons in the patient's body and the spatial response of the collimator and detector. Advances in computer power have prompted the use of iterative reconstruction algorithms. As described by the Institute of Medicine [NRC 1996], a typical algorithm starts with an initial image estimate of $f(x, y)$, from which projections $p_\theta(t)$ are generated mathematically, based on the imaging process. Calculated and measured projections are compared and various statistical processes are used to update the image estimate and the process is repeated until differences between measured and generated projections meet acceptance criteria. A favored statistical process is the expectation maximum–maximum likelihood (EM-ML) algorithm.

14.1.7   Positron Emission Tomography (PET)

As early as the 1950s there was the realization that radionuclides emitting positrons offered enhanced medical imaging possibilities over those of SPECT. The emitted positron, within at most a few mm in tissue, annihilates with an ambient electron producing simultaneously two annihilation photons, equal in energy (0.511 MeV) and, most importantly, moving in almost opposite directions. It was recognized that detection of these photons, using the property that they are emitted simultaneously in opposite directions, would permit description, in three dimensions, of the distribution of the radionuclides in the body. Decades of development have given us positron emission tomography (PET), an indispensable tool in medical diagnosis and physiologic imaging. PET is very similar to SPECT in how images are reconstructed; however, the use of two detectors on opposite sides of the patient with coincidence photon detection logic allows finer spatial resolution of the emission location in the patient than does SPECT and, hence, better tomographic image reconstruction of the activity distribution in the patient.

PET imaging was first undertaken in the late 1960s, with imaging of a single plane per acquisition and requiring patient repositioning between acquisitions. By the late 1990s, PET scanners were available with more than 18,000 independent scintillation crystals, capable of imaging three-dimensional object regions 6-in. axially and 23-in. transversely, with resolution better than 5 mm in both directions.

Table 14.3. Characteristics of radionuclides used for PET.

Nuclide	E_{max} (MeV)	E_{av} (MeV)	Frequency	Half-life	Production Reaction
^{11}C	0.960	0.386	0.998	20.5 m	^{14}N(p,α)
^{13}N	1.199	0.492	0.998	9.97 m	^{16}O(p,α),^{13}C(p,n)
^{15}O	1.732	0.735	0.999	122 s	^{15}N(p,n)
^{18}F	0.634	0.250	1.000	110 m	^{18}O(p,n)

Principles

Positrons have but a fleeting existence as anti-matter, usually coming to rest before annihilating with an electron. The annihilation produces two 0.511-MeV photons traveling exactly in opposite direction. Rarely, annihilation may occur in flight, resulting in slight deviations in the colinearity of photon emission and subsequent loss in resolution on the order of 1 mm. Positrons have a very short path in tissue as they come to rest. For example, a 1-MeV positron has a path length of about
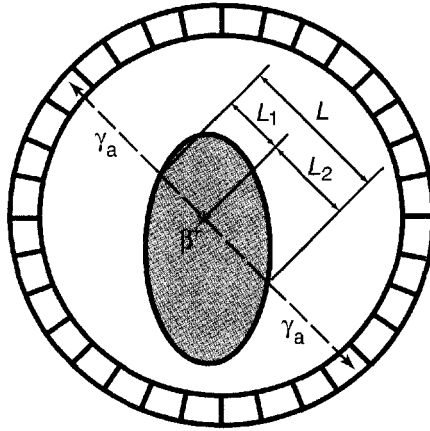
Figure 14.11. PET imaging of an object surrounded by a ring of detectors. Annihilation photons γ_a are recorded by detectors on opposite sides of the ring, and the relative intensities allow determination of the mass thickness of the distances L_1 and L_2 in the patient through which these photons travel.

4 mm. The radionuclide ^{18}F, the most frequently used isotope for PET, emits positrons with an average energy of 0.25 MeV, which have a range of less than 1 mm. Characteristics of ^{18}F and other useful positron emitters are listed in Table 14.3. All these emitters are short lived, only ^{18}F having a sufficiently long life to permit transport of radiopharmaceuticals to sites a few hours from the point of preparation. These radionuclides are normally produced by cyclotrons. A typical cyclotron (Siemens/CTI RDS 112) uses a beam of 11-MeV negative hydrogen ions to induce the nuclear reactions listed in the table.

Annihilation photons leaving the body are detected by an array of detectors that surround the patient, as shown in Fig. 14.11, which illustrates imaging in the plane of the paper. Events are recorded only when two detectors each detect an annihilation photon simultaneously, i.e., within 10 to 25 ns of each other. Events separated further in time are not recorded. The line joining the two recording detectors is a *line of response* (LOR) along which the annihilation photons have traveled and on which the positron decay occurred. This coincident detection technique allows a determination of the direction of the annihilation photons without the physical collimation needed in SPECT. For this reason coincident detection is often called electronic collimation.

Along a given LOR (see Fig. 14.11), the attenuation factor, i.e., the reduction in probability of detecting positron emission due to scattering or absorption of one or both the annihilation photons, is given by

$$A = \exp\left(-\oint_{L_1} ds\,\mu(s)\right)\exp\left(-\oint_{L_2} ds\,\mu(s)\right) = \exp\left(-\oint_{L} ds\,\mu(s)\right), \quad (14.19)$$

in which μ is the total linear interaction coefficient for 0.511-MeV photons. Thus

we see that the attenuation factor is the same no matter where on the LOR the positron decay occurs. Although, with knowledge of the anatomy of the patient being imaged, it would be possible to compute the attenuation factor for each LOR, measured attenuation factors are preferred. One method, for example, uses, within the detector ring, a rotating source of annihilation photons, such as an equilibrium mixture of ^{68}Ge and ^{68}Ga, to collect blank scans with and without the patient present. Attenuation factors for each LOR may be derived from these scans and applied to scans of the patient containing positron-emitting radiopharmaceuticals.

The total number of coincidence events recorded by a given pair of detectors, corrected by the appropriate attenuation factor between the detectors, is a measure of the activity in the patient integrated along the LOR between the detectors. From a complete set of such line integrals of the activity between all pairs of detectors surrounding a patient, the activity distribution within the plane of the detector ring can be reconstructed using methods similar to those used in CT image reconstruction.

PET Detectors

Detectors used for annihilation coincidence counting must be small because their size defines the resolution of the scanner. To improve sensitivity, they must present a high photoelectric cross section for 0.511-MeV photons and a high scintillation output (fluorescence efficiency). For these reasons, bismuth germanate (BGO) or lutetium oxyorthosilicate (LSO) have largely replaced sodium iodide as scintillator crystals for PET. For annihilation photons, bismuth has a photoelectric cross section about seven times that of iodine and BGO has a density twice that of NaI although a lower fluorescence efficiency. However, while lutetium has a cross section only half that of bismuth, LSO has an fluorescent efficiency five times that of BGO.

Figure 14.12 shows the organization of the ring of scintillation detectors in a modern PET scanner (GE PET Advance). In the ring are 56 modules circumferentially, each supplied with its own electronics package. In each module there are six detector blocks, each consisting of a 6 by 6 array of BGO crystals, for a total of 12,096 crystals. As illustrated in Fig. 14.13, each block of 36 crystals is observed by two dual photomultiplier tubes (PMT). By a weighted average of signals from the PMTs, the position of an absorption event in the block may be determined. There are thus 18 direct image planes axially, each 8.5 mm wide, giving an axial field of view of 15 cm. Other characteristics of the GE Advance scanner, along with characteristics of the Siemens ECAT scanner are listed in Table 14.4.

In multi-ring systems such as the GE and Siemens scanners, sensitivity may be improved by accepting coincidences not only for detectors within the same ring but also for detectors in adjacent rings, even across several rings. In the Advance scanner, for example, there are 18 direct planes and 17 crossed planes, for a total of 35 planes over the 153 mm axial field of view. Axial and transaxial resolution are thus about the same, 4.8 mm.

Applications

PET is ideally suited to generating images that reveal physiology. As we have seen, low-Z radionuclides are rich in positron emitters, which are easily substituted into molecules such as water, glucose, ammonia, etc. that move through metabolism and circulation within the human body. There are two broad avenues of application.
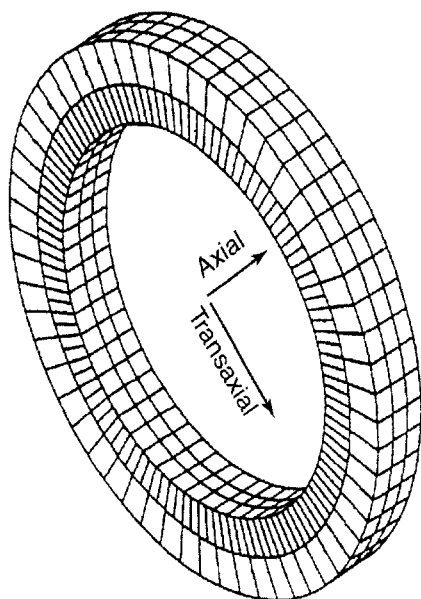
Figure 14.12. Ring structure for the GE Advance PET scanner showing the 336 detector blocks.
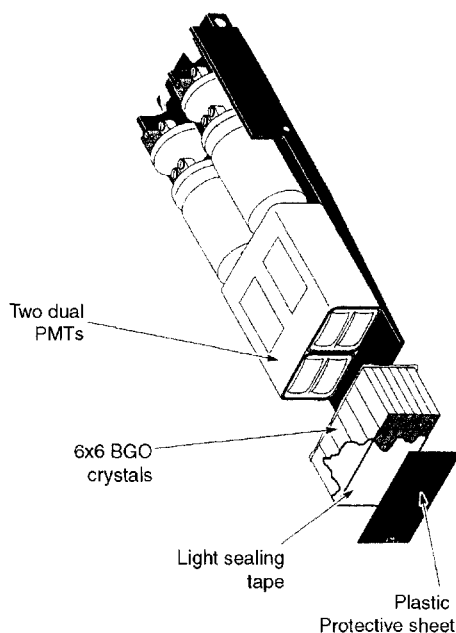
Figure 14.13. Detector block structure for the GE Advance PET scanner. Each block contains 36 BGO detector cystals.

Table 14.4. Comparison of PET scanner features.

Characteristic	Siemens ECAT Exact	GE Advance
Detector material	BGO	BGO
Crystal dimensions (mm)	6.75 x 6.75 x 20	4 x 8.5 x 30
Crystals per detector	64	36
PM tubes per detector	4	4
Detector ring dia. (mm)	824	939
Number of rings	24	18
Number of crystrals	9,216	12,096
Axial field of view (mm)	162	153
Portal diameter (mm)	562	590

One is studies of changes in brain stimulation and cognitive activation associated with Alzheimer's disease, Parkinson's disease, epilepsy, and coronary artery disease. The other is location of tumors and metastases in the brain, breast, lung, and gastrointestinal system. PET is distinguished by its very great sensitivity, allowing display of nanomolar trace concentrations.

Examples of PET Images

Figure 14.14 shows results of two whole-body PET scans of cancer patients. One panel of images is for a lung-cancer patient, the other for a lymphoma patient. In each panel, from top to bottom, are views of coronal, axial, and sagittal slices. Dark regions, displaying excess radiopharmaceutical activity, identify uptake by cancer cells. Images were obtained using the GE Advance PET Scanner. In each case, patients were administered approximately 10 mCi of [^{18}F] 2-fluoro-2-deoxy-d-glucose (FDG).

Figure 14.15 illustrates use of combined imaging techniques in cancer diagnosis and treatment planning. The patient had a known right lung mass. The diagnostic problem addressed by the imaging procedure was whether the tumor had invaded the mediastinum (chest wall). The left image is a transverse CT slice through the thorax. The central image is a PET image in geometric registration with the CT image. The right image displays merger of the CT and PET scans. With the CT scan alone, it is difficult to distinguish the extent of tumor invasion. With the PET scan alone, the tumor is evident, but anatomical information is lacking. The combined image on the right, drawing on the strengths of both CT and PET, reveals that the tumor does not invade the chest wall. Other examples, and details of the procedure for superimposing PET and CT images are discussed in a paper by Yu, Fahey, and Harkness [1995].

14.1.8   Magnetic Resonance Imaging (MRI)

Magnetic resonance imaging (MRI), based on the phenomenon of nuclear magnetic resonance, produces high quality images of the soft tissues of the human body.[2] Initially a tomographic technique, MRI is now capable of slice images in any orientation as well as three dimensional and cinematographic imaging. MRI is used not only for anatomical imaging but also for functional studies of blood flow and neurological activity. Although it does not involve radioactive nuclides or nuclear radiation, it depends critically on the spin (angular momentum) properties of the atomic nucleus. Thus, its inclusion in this chapter of applications of nuclear technology.

Historical Development

Working independently, Felix Bloch and Edward Purcell discovered nuclear magnetic resonance phenomena in 1946 for which they were awarded the Nobel Prize in 1952. Although NMR was first used for chemical and physical molecular analysis, it was shown in 1971 by Raymond Damadian that different tissues, normal

---

[2]The MRI technique has undergone a significant acronym and name change since its discovery. Initially, it was called nuclear magnetic resonance imaging (NMRI) or nuclear magnetic resonance computerized tomography (NMR-CT); but the word "nuclear" has since been thought to be unsettling to many patients, and this word has now been eliminated, even though the technique fundamentally relies on nuclear magnetic properties.
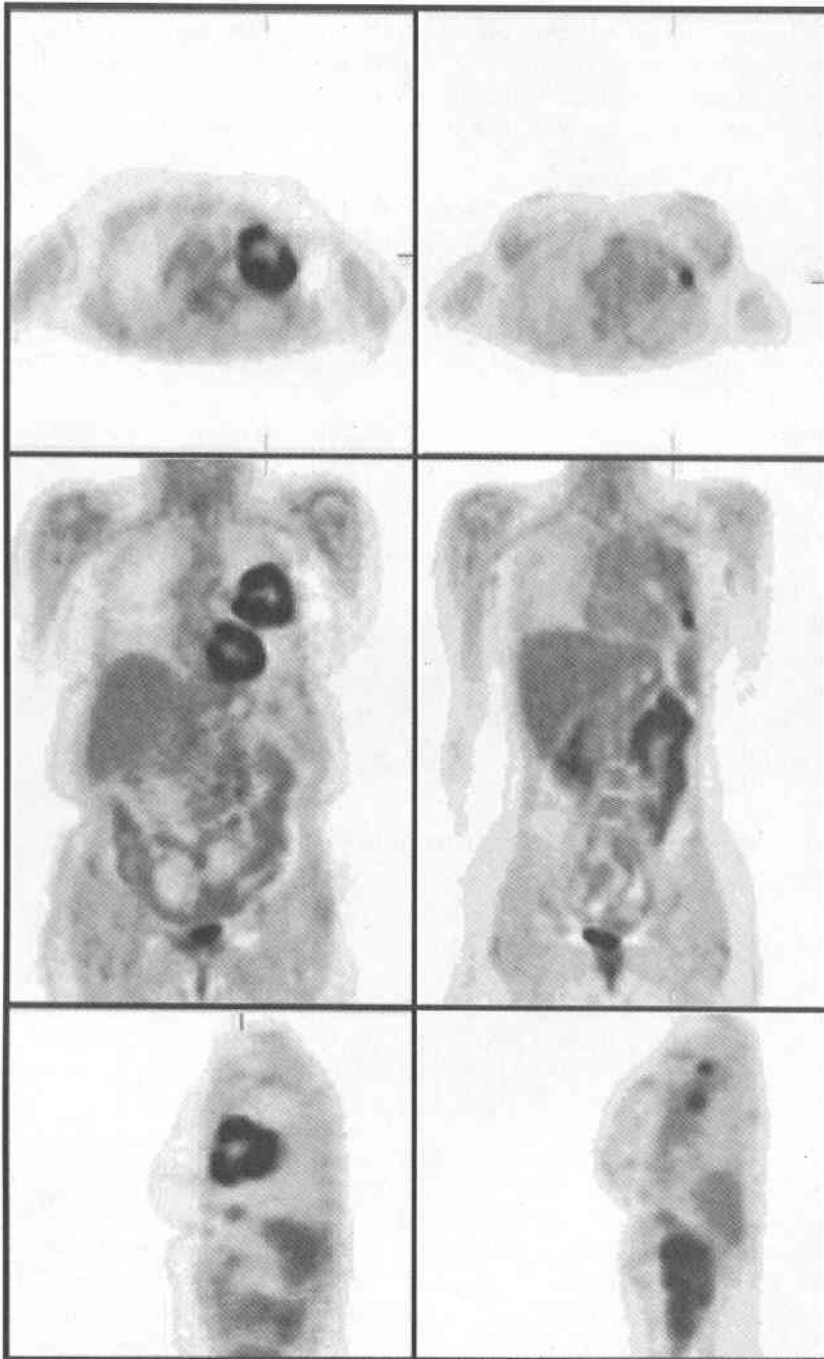
Figure 14.14. PET images of cancer patients. Left panel: lung cancer. Right panel: lymphoma. Illustration courtesy of Dr. Frederic H. Fahey, Wake Forest University Baptist Medical Center.
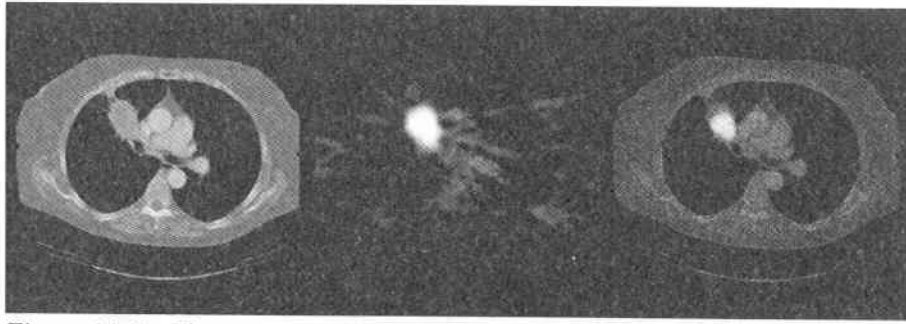
Figure 14.15. Thorax images of patient with right lung mass. Left: CT, Center: PET, Right: PET and CT images superimposed. Illustration courtesy of Dr. Frederic H. Fahey, Wake Forest University Baptist Medical Center.

and abnormal, showed differing nuclear magnetic responses. This, and the 1973 discovery of computed tomography (CT) opened the way for use of MRI in the diagnosis of disease. Magnetic resonance imaging was first demonstrated in 1973 by Paul Lauterbur who used a back projection technique similar to that used in x-ray CT. In 1975 Richard Ernst proposed magnetic resonance imaging using phase and frequency encoding together with the Fourier image reconstruction technique, the basis of current MRI techniques. In 1977, Raymond Damadian demonstrated MRI of the whole body and, in the same year, Peter Mansfield developed the echo-planar imaging (EPI) technique. Edelstein and coworkers demonstrated imaging of the body using Ernst's technique in 1980, and showed that a single image could be acquired in approximately five minutes by this technique. By 1986, the imaging time was reduced to about five seconds. In 1987 echo-planar imaging was used to perform real-time movie imaging of a single cardiac cycle. In this same year, Charles Dumoulin was perfecting magnetic resonance angiography (MRA), which allowed imaging of flowing blood without the use of contrast agents. In 1991, Richard Ernst was awarded the Nobel Prize in Chemistry for his achievements in pulsed Fourier transform NMR and MRI. In 1993 functional MRI (fMRI) was developed, allowing the functional mapping of the various regions of the human brain. Advances in the capabilities of MRI are a continuing area of research.

Principles

All nuclei with an odd number of neutrons and/or protons possess an intrinsic angular momentum (spin) and, consequently, a magnetic moment. In the presence of a strong magnetic field, such nuclei experience a torque and tend to align either in a parallel or antiparallel direction to the magnetic field. The spinning nuclei respond to a strong external magnetic field by precessing around the direction of the field much like the spin axis of a gyroscope precesses around the direction of the gravitation field. The precession frequency is directly proportional to the magnetic field strength H_o and is unique to each nuclear species. A precessing nucleus has two possible orientations each with a slight difference in energy: in the lowest energy state the nuclear spin precesses around the direction of the external magnetic field (parallel), and in a slightly higher energy state, the nuclear spin precesses around the

direction opposite the magnetic field (antiparallel). The difference between these two energy states is $2\mu H_o$ where μ is the nuclear magnetic moment. For protons in a magnetic field of 0.5 to 20 kG, this energy difference is relatively small, typically that of photons in the radio frequency (RF) range (2 to 85 MHz).

In MRI, the patient is placed in a large static magnetic field, often produced by a superconducting magnetic. This field causes the nuclei to align and precess about the magnetic field in their lowest (parallel) energy state. A pulse of electromagnetic energy provided by an RF magnetic field causes many of the aligned nuclei to flip to the higher energy state in which they precess antiparallel to the static magnetic field. The excited precessing nuclei then spontaneously return or relax to their lower energy state by emitting RF photons which can be detected by the same RF coils used to produce the RF pulse that originally excited the spinning nuclei. It is empirically observed that the relaxation times are sensitive to the molecular structures and environments surrounding the nuclei. For example, average proton relaxation times in normal tissue are significantly less than in many malignant tissues. The strength of RF signal emitted by relaxing nuclei also depends on the density of precessing nuclei or the spin density. Thus, in MRI, magnetic field gradients are also applied, in addition to the large uniform static field H_o, to resolve the spatial distribution of spin densities. The different spin relaxation times of materials and the ability to measure the spatial distribution of spin densities make MRI a unique and robust technique in diagnostic imaging. An example MRI result is shown in Fig. 14.16.

MRI is unusual compared to other nuclear medicine imaging techniques in that there is a great diversity in the way data are collected and images are reconstructed. For example, MRI images can be formed by direct mappings, projection reconstruction, and Fourier imaging. Also there are many combinations of different magnetic gradient coils and magnetic field and pulse strengths that can be used. Work continues on improving and extending MRI capabilities by applying different variations in the measurement and image reconstruction technology.

14.2   Radioimmunoassay

Radioimmunoassay (RIA) is a technique utilizing radionuclides for measuring, with exquisite sensitivity, the concentration of almost any biological molecule. It was originally developed for use in studies of the human immune system in which a foreign protein (antigen) provokes an immune response causing special molecules (antibodies) to be created that chemically attach themselves to the antigen at some specific site on the antigen's surface, thereby deactivating the antigen. Today it can be used to measure concentrations of enzymes, hormones, or almost any other molecule to which antigens can be chemically attached. Measurement of concentrations as small as a few ng/ml to pg/ml can often be obtained.

RIA is extensively used today in many areas of biomedical research and diagnostic medicine. It is used in clinical chemistry, endocrinology and toxicology. In some laboratories, it finds use in tests for steroid and peptide hormones and in markers for hepatitis-B infection [Koneman et al. 1997]. It also finds use in diagnosis of histoplasmosis and streptococcus pneumonia [Rose et al. 1997]. The first use of RIA, in 1959, was for detection of insulin in human plasma [Joklik et al. 1992].
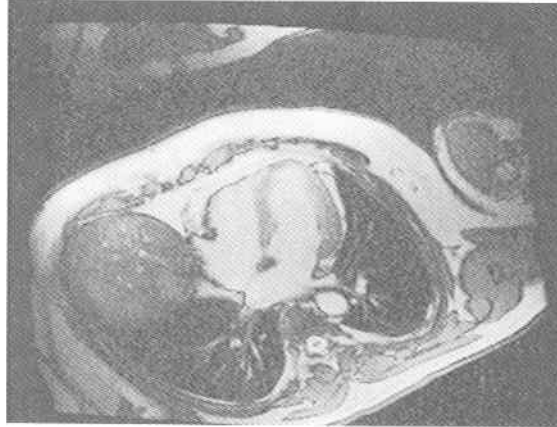
Figure 14.16. MRI image of the thorax, displaying a four-chamber view of the heart, generated using gated MRI imaging. Courtesy of Dr. Craig A. Hamilton, Wake Forest University Baptist Medical Center.

Principles

Suppose we want to measure the amount or concentration of some particular antigen in a sample. There are two basic approaches used in RIA. In *capture* RIA, we first obtain two different antibodies that attach themselves to different sites on the antigen in question. The number of both kinds of antibodies to be used in the assay is assumed to be greater than the unknown number of antigens in the sample. One of the antibody species is tagged or labelled with an radionuclide such as ^{3}H or ^{125}I. The non-radioactive antibodies are attached to a solid surface, e.g., plastic beads, polystyrene microtubes, or a substrate in a sample vial. To begin the assay, the antigens, of unknown concentration, and the solid-phase bound antibodies are mixed and incubated to allow the antigens to bind to the antibodies. The tagged antibodies are then added to the mixture and also allowed to bind to the antigens. Extraneous material is then washed away, leaving all the antigens bound to the solid material and now tagged with radioactive antibodies. The activity of the resulting complex is proportional to the number of tagged antibodies bound to the solid surface. This number equals the unknown number of antigens in the sample. By performing the same assay procedure with different *known* amounts of the antigen, a "standard" or calibration plot can be obtained that relates activity to antigen concentration. From this plot, the unknown antigen concentration is then readily determined from the measured sample activity.

In the RIA approach, known as *competitive binding* RIA, antibodies are again attached to a solid phase. The sample with the unknown amount of antigen, the antibodies attached to a solid phase, and a solution of known concentration of the same antigen that has been tagged with a radionuclide are all mixed together. The antigens, of unknown amount, in the sample being assayed and the tagged antigens, of known amount, compete in attaching themselves to the antibodies fixed to the solid surfaces. The ratio of tagged to untagged antigens eventually binding to the

antibodies equals their ratio in the initial mixture. After incubating, the sample is washed to remove unbound antigens and the activity of the antigens bound to the solid phase is measured. By performing this same procedure using the same amount of tagged antigen and varying amounts of untagged antigen, a calibration curve can be obtained relating activity to untagged antigen concentration.

Instead of using a radionuclide as a tag, enzymes can also be used to tag antigens or antibodies. This technique is referred to as enzyme-linked immunosorbent assay (ELISA) and the detection of the enzyme may be colorimetric. Whereas RIA presents difficulties in dealing with radioactive materials, it is more sensitive than ELISA and is widely used in research.

14.3 Diagnostic Radiotracers

Radioactive tracer techniques see wide use in the physical, biological, and medical sciences. Because of the ease of quantitative determination of very small quantities of a radionuclide, it is quite feasible to incorporate trace quantities of the radionuclide in reactants of a process and to measure yields, time constants, etc., by measuring activities in process intermediates and products. The first use of diagnostic radionuclides was in 1924, when George de Hevesy and, independently, Hermann Blumgart used ^{214}Bi to study circulation. The first artificially produced tracer, ^{24}Na was used in 1935 [Ice 1995]. The same year, Hevesy began using the physiologic radionuclide ^{32}P produced by bombarding ^{31}P with neutrons. For this work he received the Nobel prize in 1943. First used in 1939, with production in a cyclotron, was the nuclide ^{131}I. Later, this and a host of other radionuclides for pharmaceutical application were produced in nuclear reactors. Key among these was ^{99m}Tc. which became commercially available in 1957 through generation from a ^{99}Mo "cow." The generator was developed at Brookhaven National Laboratory and the product is ideal in half-life and gamma-ray energy. The ^{99}Mo, reactor produced, is loaded on an aluminum oxide column and the ^{99m}Tc is eluted (or "milked" from the Mo cow) using a saline solution, and is sterile and free of pyrogens. First used on humans in 1957. ^{99m}Tc is the mainstay of some 90 percent of diagnostic nuclear medicine. Other radionuclide generators include ^{68}Ge/^{68}Ga, which delivers a positron source, ^{81}Rb/^{81m}Kr, ^{82}Sr/^{82}Rb, ^{87}Y/^{87m}Sr, ^{113}Sn/^{113m}In, and ^{191}Os/^{191m}Ir [Ice 1995].

The availability of radioisotopes and the newly invented rectilinear scanner of Benedict Cassen in 1949 and the gamma-ray (scintillation) camera of Hal O. Anger in 1957 opened the way to dramatic advances in nuclear medicine during the past 50 years. A comprehensive history of the use of diagnostic radionuclides is found in the review article by Early [1995]. A comprehensive listing of radionuclides produced in North America, and their suppliers, was published by Silberstein et al. [2000].

Uptake studies and multi-compartment kinetic modeling are among the most common and most important medical applications of radioactive tracers. A good example of uptake studies is the diagnosis of hyperthyroidism, most commonly Graves' disease, which involves abnormal release of thyroid hormones. Abnormal iodine uptake in the thyroid may be determined by measurement of ^{123}I or ^{131}I using a radiation detector such as a NaI scintillation counter external to the body in the thyroid region of the neck.

The ICRP Report 53 [1988] on the use of radiopharmaceuticals lists 75 radionu-

Table 14.5. Selected examples of tracers used in nuclear medicine. From Sorenson and Phelps [1987].

Process	Tracer
Blood Flow	
Diffusable	^{133}Xe, ^{15}O, [^{11}C]alcohols, CH_3^{18}F
Non-Diffusable	[^{99m}Tc]macroaggregated albumin microspheres
Blood Volume	
Red Cells (RBC)	[^{99m}Tc]-, [^{51}Cr]-,[^{15}CO]-RBC
Plasma	[^{125}I]-, [^{111}C]-albumin
Transport/Metabolism	
Oxygen	[^{15}O]O_2
Glucose	2-deoxy-2-[^{18}F]fluoro-D-glucose, etc.
Protein Synthesis	L-[1-^{11}C]leucine,-methionine, etc.

clides used in tracer studies. The most commonly used radionuclide is ^{99m}Tc. Next most common are the ^{123}I, ^{125}I, and ^{131}I isotopes of iodine. Some two dozen radiopharmaceuticals are listed for ^{99m}Tc, ranging from sulfur colloids used for liver studies and polyphosphates used for bone scans. Some example radiopharmaceutical tracers and their applications are given in Table 14.5.

14.4 Radioimmunoscintigraphy

The radioimmunoscintigraphy technique, abbreviated RIS, employs radiolabeled antibodies to image and characterize disease *in vivo*. The technique is used for malignant pathology as well as benign, e.g., myocardial infarction. In RIS, a radiolabeled monoclonal antibody is targeted to a particular line of cells such as tumor cells. Gamma-ray camera, PET, or SPECT techniques are then used image the spatial distribution of the radionuclide, and hence the pathology of interest.

Several factors are required [Britton & Granowska 1998]: The antibody must be capable of detecting the cancer; the radionuclide must be capable of being imaged; and a radiolabeling method suitable for human use must be available. The production of a pure antibody against a selected antigen has been made possible through the development of monoclonal antibody (Moab) technology. Mettler and Guiberteau [1998] describe the production of monoclonal antibodies as follows: An animal such as a mouse is immunized with the antigen. In the animal, B lymphocytes begin producing antibodies. These are harvested and mixed with mouse myeloma cells. Fusion of the myeloma cells with the B lymphocytes produces a hybridoma which can continue producing antigen-specific antibodies and can perpetuate itself. The hybridomas are cloned, from which one is selected that produces the antibody of interest. The antibodies are then purified and labeled.

14.5 Radiation Therapy

Nuclear therapeutic medicine had its beginnings with Marie and Pierre Curie's discovery in 1898 of radioactive polonium and radium and with Roentgen's discovery in 1896 of x rays. These events, and a thorough review of the history of therapeutic

nuclear medicine are found in the review articles by Early and Landa [1995] and Coursey and Nath [2000]. Here we mention only a few highlights of the very early uses of radioactivity and nuclear radiation.

14.5.1   Early Applications
X-Ray Therapy
The first therapeutic uses of x rays took place in 1896, shortly after Roentgen's discovery. As described by Orton [1995], Grubbe, in Chicago, treated breast cancer, Voight in Germany, treated nasopharyngeal cancer, and Despeignes, in France, treated stomach cancer. The first successful therapeutic uses were in Sweden in 1899, in treatments of both squamous-cell and basal-cell skin cancer. Early x ray tubes were not standardized and were largely unfiltered, resulting in excessive skin doses. Dose fractionation was used, but only for the convenience of the patient or physician, not for scientific reasons. The work of Bergonié and Tribondeau in 1906 showed that cancer cells were most susceptible to destruction by radiation if in the process of mitosis. This led to the expectation that a fractionated dose would be much more effective than a single dose, but many years would pass before dose fractionation was applied scientifically.

Radionuclide Therapy
Until about 1950. only ^{226}Ra and ^{222}Rn saw use for therapy. First used for treatment of skin lesions in 1900 and cancer therapy in 1903, by 1920 radium was being used for treatment of lung cancer, using a sealed source in the thoracic cavity. Sealed 10-100 mg sources of ^{226}Ra were used near the skin or within body cavities. Gaseous ^{222}Rn, daughter product of ^{226}Ra, was first used in 1914, sealed in glass capillary tubes. In later years, the long-lived radium was used in fixed installations as a generator for the short-lived radon.

By the late 1920s, ^{226}Ra was used in treatment of deep lying tumors. This practice continued until the 1950s, when ^{60}Co, ^{198}Au, and ^{192}Ir became available.

Internal Therapy
The exploitation of radium and radon in the first few decades after discovery was a disgraceful display of quackery and excess. These radionuclides were misused in treatment of a host of ailments and conditions ranging from barber's itch to hemorrhoids. Only in the 1930s, after some well publicized deaths from misuse of radiation sources, and after the health effects of radium on the World War I radium dial painters were made known, were efforts made to regulate and control radium use. The Department of Agriculture, the Federal Trade Commission, and the American Medical Association led the way. Nevertheless, well into the 1980s, appliances containing uranium were being promoted as agents for arthritis cures.

14.5.2   Teletherapy
The use of beams of radiation to destroy malignant growths and other lesions has a long history. Many types of radiation, all generated externally to the patient, can be used.

In 1913, William D. Coolidge invented the tungsten-anode, vacuum x-ray tube. This Coolidge tube was the prototype of modern x-ray tubes and allowed standardization and reliable dosimetry and treatment planning. Higher energy x-ray

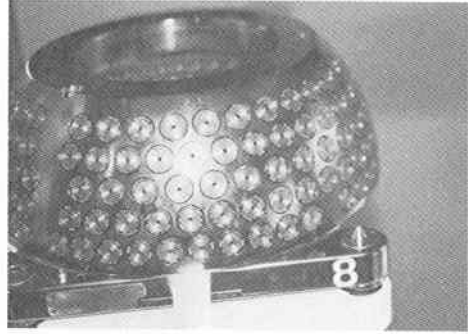**Figure 14.17.** Leksell Gamma Knife for stereotactic radiosurgery.

Figure 14.18. Close-up view of the collimator helmet for the Leksell Gamma Knife.

machines were introduced in the 1920s, with 80 to 140-kVp units common. Depth-dose tables and isodose curves greatly improved treatment planning. Ionization dosimetry was introduced and the Roentgen unit of radiation exposure was established in 1928. The 1930s saw 500-kVp units introduced in 1934. In 1937, 1.25-MeV Van de Graaf accelerator sources came into use. The greater depth of penetration of the higher energy x rays, and the application of fractionation, improved treatment and avoided severe damage to superficial tissues.

In the 1960s intense beams of gamma rays produced by high activity radionuclide sources were used also for teletherapy. ^{60}Co was the radioisotope most frequently used. It emits 1.17 and 1.25-MeV gamma rays and can be produced in quantity in a nuclear reactor. Teletherapy devices with many kCi of ^{60}Co in a rotating head which, through careful collimation and filtering, could produce an intense beam of gamma rays came into widespread use.

Linear accelerators were pioneered in the 1930s and, by the 1980s, became the standard sources of x rays for radiation therapy in developed countries, largely replacing ^{60}Co units. Common are machines with lower energies ranging from 4 to 6 MeV and upper energies ranging from 10 to 20 MeV. Multi-leaf collimators came into use in the 1990s, as did lower-energy treatment simulators used in the design and testing of patient-specific collimators. Spiral CT scanners, with three-dimensional imaging, are now used for treatment-specific collimation and dosimetry planning. Figure 14.7 shows such a scanner.

A very special type of beam therapy is *stereotactic radiosurgery*. Small lesions in the brain are treated with the use of multiple, non-coplanar beams of gamma rays focused to a very small region. High precision is required in the positioning of the patient, and CT scans are used for treatment planning. Figures 14.17 and 14.18 show the Leksell Gamma Knife, which delivers highly accurate external radiation to intracranial structures from an array of collimated beams of ionizing radiation. The Knife utilizes a single dose of radiation directed through the 201 ports of a collimator helmet to the target within the brain. During irradiation there are no moving parts within the Knife and therefore safety, stability and accuracy are inherent features.

14.5.3 Radionuclide Therapy

In the United States alone, hundreds of thousands of patients annually receive therapy using radionuclides. In many cases, sealed sources are used, often in the close proximity of cancers for treatment purposes, and sometimes for short-range treatment of other conditions. In other cases, unsealed sources are ingested or injected in a form as to be concentrated in cancer tissue, and thereby attacking cancer cells from within the affected tissue. Maisey et al. [1998] and Coursey and Nath [2000] are good sources of information on radionuclide therapy and The AAPM [2001] has published a primer on the subject.

Direct Radionuclide Therapy

A good example of the use of a radionuclide in therapy involves the treatment of thyroid disease. Iodine entering the bloodstream either directly or after ingestion is strongly concentrated in the thyroid and radioactive iodine, commonly ^{131}I, is used to ablate all or a part of the thyroid in treatment of thyrotoxicosis, goiter, or thyroid cancer. Other examples include the use of beta-particle emitters such as ^{32}P or ^{90}Y in the ablation of the synovial lining in the treatment of synovial disease. A common palliative use of beta-particle emitters such as ^{32}P and ^{89}Sr is found in the treatment of cancer metasteses in bone. The radiation dose causes both tumor shrinkage and hormonal mechanisms of pain reduction.

Radioimmunotherapy

In this technique, called RIT, a radiolabeled monoclonal antibody is targeted to a particular line of tumor cells. The antibody is produced as described in Section 14.4. The radionuclide is attached to the antibody or a smaller protein fragment. In the attachment, the radionuclide is first chemically bound to a small precursor molecule called a ligand. The ligand is then attached to the antibody, which is then injected into the bloodstream. Coursey and Nath [2000] characterize candidate radionuclides. The mainstays are beta-particle emitters ^{131}I and ^{90}Y. In many instances, nuclides emitting short-range radiations are required. Among these are alpha-particle emitters such as ^{211}At, ^{225}Ac, ^{213}Bi, and ^{212}Bi, and Auger-electron emitters such as ^{125}I and ^{111}In.

14.5.4 Clinical Brachytherapy

In brachytherapy, or short-distance therapy, sealed radiation sources are placed in or near tumors. They may be placed in fixtures outside the skin, implanted in tissues (interstitial treatment), or placed in body cavities (intra-cavity treatment). In brachytherapy planning, source configurations are determined using dummy sources, with actual sources emplaced later. This procedure, which limits personnel doses, is known as *afterloading*. There are several advantages of brachytherapy over beam therapy. Lower energy and lower strength sources can be used, leading to precise control of the spatial distribution of radiation dose. Furthermore, using longer irradiation times allows treatment over several days during which cancer cells pass through each phase of the cell cycle. This assures that each cell is treated during the more radiosensitive phases of the cycle.

Common Therapies

Sealed radium or radon sources were among the first sources used in interstitial treatment of solid tumors of many types. Intra-cavity treatments for uterine, rectal, and gynecological cancer make use of sources such as ^{137}Cs and ^{192}Ir. Each year in the United States, some 10,000 males are treated for prostate cancer interstitially using sources such as ^{125}I and ^{103}Pd. Some 60 to 100 "seeds" containing these radionuclides are surgically implanted in the prostate [Coursey and Nath 2000].

Intravascular Therapy

Balloon angioplasty, used to open occluded arteries, is one form of brachytherapy. In the procedure, artery walls may be damaged and in the healing process the artery walls may reclose, a phenomenon called restenosis. This may be minimized by applying a radiation dose to arterial lesions using catheter-borne radiation sources. Similarly, arterial stents may incorporate radiation sources in the stent material to minimize restenosis.

14.5.5   Boron Neutron Capture Therapy

This therapy, called BNCT, is a hybrid or binary therapy, employing a beam of radiation to generate an interstitial source of highly ionizing radiation within cancer cells. The therapy has reached the stage of clinical trials for treatment of glioblastoma multiforme (GBM), the most highly malignant and persistent of brain tumors.

In 1936 G.L. Locher introduced the concept of neutron capture therapy (NCT), i.e., introduction into a tumor of an element that reacts with particles in an incident radiation beam to produce short-range secondary charged particles capable of cell destruction. Boron, and the reaction ^{10}B(n,α)^{7}Li, or lithium, and the reaction ^{7}Li(p,n)^{7}Be, are possible candidates. In 1952 Sweet suggested that the boron reaction might be useful in the treatment of GBM.

In the treatment of GBM, a drug such as borocaptate sodium (BCS) is used to transfer boron through the blood-brain barrier to tumor cells. The barrier protects normal brain cells from blood-borne substances but is ineffective in tumor cells. The patients head is irradiated by a beam of epithermal neutrons, ideally with energies sufficient to assure that the neutrons are just thermalized as they reach the glioblastoma. The nuclear reaction produces an alpha particle of energy about 1.5 MeV and a ^{7}Li atom of energy about 0.84 MeV. These charged particles give up their energy in tracks only about one cell diameter in length. They are thus very effective in destruction of tumor cells. Unfortunately, blood-vessel walls are also damaged by pruducts of the (n,α) reactions, and this damage places a limit on the dose that can be delivered to tumor cells.

ACKNOWLEDGMENT

BIBLIOGRAPHY

AAPM, "A Primer for Radioimmunotherapy and Radionuclide Therapy," Report 71, American Association of Physicists in Medicine, Medical Physics Publishing, Madison, Wisconsin (2001).

BRITTON, K.E., AND M. GRANOWSKA, "Radioimmunoscintigraphy," in *Clinical Nuclear Medicine*, 3d. ed., M.N. MAISY, K.E. BRITTON, AND, B.D. COLLIER, eds., Chapman & Hall Medical Publishers, London (1998).

COURSEY, B.M., AND R. NATH, "Radionuclide Therapy," *Physics Today*, April, 2000, pp. 25-30.

EARLY, P.J., "Use of Diagnostic Radionuclides in Medicine," *Health Physics* **69**: 649-661 (1995).

EARLY, P.J., AND E.R. LANDA, "Use of Therapeutic Radionuclides in Medicine," *Health Physics* **69**: 677-694 (1995).

FEWELL, T.R., R.E. SHUPING, AND K.R. HAWKINS, *Handbook of Computed Tomography X-Ray Spectra*, HHS (FDA) 81-8162, U.S. Department of Health and Human Services, Food and Drug Administration, Rockville, MD, 1981.

HENDEE, W.R., "History and Status of X-Ray Mammography," *Health Physics* **69**: 636-648 (1995).

HIRIYANNAIAH, H.P., "X-ray Computed Tomography for Medical Imaging," *IEEE Signal Processing Magazine*, March 1997.

ICE, R.D., "History of Medical Radionuclide Production," *Health Physics* **69**: 721-727 (1995).

ICRP, *Radiation Dose to Patients from Radiopharmaceuticals*, Report 53, International Commission on Radiological Protection, Pergamon Press, Oxford, 1988.

ICRU, *Radiation Dosimetry: X Rays Generated at Potentials of 5 to 150 kV*, Report 17, International Commission on Radiation Units and Measurements, Washington, DC, 1970.

JOKLIK, W.K., et al. (Eds.) *Zinsser Microbiology*, 20th. Ed., Appleton & Lange, Norwalk. CT, 1992.

KAELBLE, E.F. (Ed.), *Handbook of X Rays*, McGraw-Hill, New York, 1967.

KAK, A.C., AND M. SLANEY, *Principles of Computerized Tomographic Imaging*, IEEE Press, New York, 1988.

KONEMAN, E.W. et al., *Color Atlas and Textbook of Diagnostic Microbiology*, 5th. Ed., Lippincott, Philadelphia, 1997.

LEONDES, C.T. (Ed.), *Medical Imaging Systems Techniques and Applications: Modalities,*, Gordon & Breach, Amsterdam, 1997.

METTLER, F.A., AND M.J. GUIBERTEAU, *Essentials of Nuclear Medicine Imaging*, 4th. ed., W.B. Saunders, Philadelphia (1998).

MAISEY, M.N., K.E. BRITTON AND, B.D. COLLIER, (Eds.), *Clinical Nuclear Medicine*, Chapman & Hall, London 1998.

NAS, *The Effects on Populations of Exposure to Low Levels of Ionizing radiation*, Report of the BEIR Committee, National Research Council, National Academy of Sciences, Washington, D.C., 1980.

NRC, National Research Council, Institute of Medicine, *Mathematics and Physics of Emerging Biomedical Imaging*, National Academy Press, Washington, D.C., 1996.

ORTON, C.G., "Uses of Therapeutic X Rays in Medicine," *Health Physics* **69**: 662-676 (1995).

ROSE, N.R., et al. (Eds.) *Manual of Clinical Immunology*, 5th Ed., American Society for Microbiology, Washington, D.C., 1997.

SILBERSTEIN, E.B., et al., "Availability of Radioisotopes Produced in North America", *J Nucl Med* **41**: 10N-13N (2000).

SORENSON, J.A., AND M.E. PHELPS, *Physics in Nuclear Medicine*, 2nd ed., W.B. Saunders Company, Philadelphia, 1987.

UN, *Sources and Effects of Ionizing Radiation, Vol. I: Sources, Vol. II: Effects*, United Nations Scientific Committee on the Effects of Atomic Radiation, UNSCEAR 2000 Report to the General Assembly, with Scientific Annexes, United Nations, New York, NY, 2000.

YU, J.,N., FAHEY, F.H., HARKNESS, B.A., et al., "Intermodality, Retrospective Image Registration in the Thorax," *J Nucl Med* **36**: 2333-2338 (1995).

WEBSTER, E.W., "X Rays in Diagnostic Radiology," *Health Physics* **69**: 610-635 (1995).

PROBLEMS

1. Relate a personal experience with a diagnostic-radiology or nuclear-medicine procedure. Were risks and benefits of the procedure explained to you? Were you given information about radiation doses associated with the procedure? In reading this chapter, have you gained a better understanding of the procedure? What insights have been gained and what new questions have come to mind?

2. Consider the two x-ray spectra depicted in Fig. 14.2 produced by the same x-ray machine. Explain why the spectra are shifted in energy.

3. Consider an x-ray examination of bone, approximated as a 2-cm diameter cylinder. In the image, what is the bone's range of *subject contrast* for 100-keV x rays? Explain why the *image contrast* of the bone is less than the subject contrast. What can be done to improve the image contrast?

4. Many source and detector configurations can be used in x-ray tomography. Explain how the machine design is influenced by (a) minimizing costs, (b) increasing image resolution, (c) minimizing patient exposure, (d) minimizing the exposure time, (e) and increasing image contrast.

5. Why is ^{99m}Tc useful in diagnostic nuclear medicine but not therapeutic? Describe how decay characteristics such as half-life, atomic number, type of radiation, and energy of radiation affect the choice of a radionuclide for a particular nuclear-medicine procedure.

6. Explain why positron-emitting isotopes are not usually produced in nuclear reactors.

7. To treat thyroid cancer ^{131}I is injected in the patient where it rapidly accumulates in the thyroid. ^{131}I with a half-life of 8.0 d emits beta particles with an average energy of 182 keV/decay and gamma rays with an average energy of 382 keV/decay. In addition, ^{131}I has a biological half-life in the thyroid of 4.1 d. (a) What is the effective half-life of ^{131}I in the thyroid. (b) How many millicuries of this radioisotope should be injected to deliver a 250 Gy dose to the 20-gram thyroid?

8. Explain why SPECT must use a physical collimator, while PET has no need of such a collimator. Also explain what determines the image resolution in both procedures.

9. Explain why nuclear wastes *per unit activity* is of less societal *and* physical concern for medical applications than those produced in nuclear power plants.